Available online at www.sciencedirect.com
ScienceDirect
Journal of Power Sources 173 (2007) 788–794
JOURNAL OF POWER SOURCES
www.elsevier.com/locate/jpowsour

Effects of ageing on defect structure in the Bi_3NbO_7–Bi_3YO_6 system

I. Abrahams [a,*], F. Krok [b,**], A. Kozanecka-Szmigiel [b], W. Wrobel [b], S.C.M. Chan [a], J.R. Dygas [b]

[a] *Centre for Materials Research, School of Biological and Chemical Sciences, Queen Mary, University of London, Mile End Road, London E1 4NS, United Kingdom*
[b] *Faculty of Physics, Warsaw University of Technology, ul. Koszykowa 75, 00-662 Warsaw, Poland*

Available online 21 May 2007

Abstract

Ageing effects in the defect fluorite structure of $Bi_3Nb_{1-x}Y_xO_{7-x}$ have been studied using powder neutron diffraction. Two compositions at $x = 0.4$ and $x = 0.6$ were studied after annealing for prolonged times (400–500 h) at 410 and 550 °C. The results show that significant changes in oxide ion distribution occur at 550 °C, but that at 410 °C only the lower x-value composition exhibited such a change. A comparison of lattice parameter variation with temperature for annealed and unannealed samples suggests that at higher temperatures the oxide ion distribution is independent of thermal history.

Keywords: Bismuth oxide; Fluorite; Defect structure; Neutron diffraction; Ageing

1. Introduction

Oxide ion conductors that exhibit the basic cubic fluorite structure are amongst the best known solid electrolytes and include compounds such as the stabilised zirconias and δ-Bi_2O_3. These materials show exceptionally high oxide ion conductivities due to high vacancy concentrations on the oxide ion sublattice. In the case of bismuth oxide-based electrolytes, the polarizability of the bismuth atoms enhances oxide ion mobility leading to systems with high conductivities at relatively low temperatures.

The δ-phase of Bi_2O_3 is stable only above *ca.* 730 °C to the melting point at around *ca.* 830 °C [1]. Partial substitution of Bi by other cations, particularly the rare earths, allows for stabilisation of the cubic fluorite phase to room temperature [2–7]. Substitution of Bi by Nb also results in δ-phase stabilisation. However, ordering phenomena result in complex superlattices, which are compositionally dependent [8–10]. At the ratio $3Bi_2O_3$:$1Nb_2O_5$, a compound of stoichiometry Bi_3NbO_7 is formed, that has the cubic fluorite subcell and an incommensurate supercell [11]. However, a commensurate cell has been found for $Bi_{94}Nb_{32}O_{221}$, which possesses a stoichiometry close to Bi_3NbO_7, and the structure has recently been characterised using a tetragonal supercell of dimensions $a = 11.52156(18)$ Å and $c = 38.5603(6)$ Å, in space group I-4m2 [12]. Niobium in this compound was found to be predominantly six-coordinate.

In Bi_3NbO_7, the vacancy concentration is significantly lower than that in δ-Bi_2O_3 (12.5% and 25% oxide ion vacancies per cell, respectively). It is possible to increase the vacancy concentration by subvalent substitution of Nb^{5+} in Bi_3NbO_7 and in this way approach the situation in the parent compound, δ-Bi_2O_3. We have previously examined both tetravalent (Zr^{4+} [13]) and trivalent (Y^{3+} [14,15]) substituents and have observed, in both cases, increases in conductivity with increasing vacancy concentration. In the case of the system $Bi_3Nb_{1-x}Y_xO_{7-x}$, a detailed study of the defect structure was carried out. Oxide ions were found to be distributed over three sites in the cubic Fm-3m subcell, viz: the ideal fluorite site 8c, and two other sites 32f and 48i. The distribution of oxide ion scattering over these sites was found to be compositionally dependent. At room temperature, the $x = 0$ composition was found to exhibit exclusive occupation of the 32f sites, while at $x = 1$ oxide ions were predominantly located in the 8c sites. Additionally, the oxide ion distribution was observed to be temperature dependent and was correlated with non-Arrhenius behaviour in electrical conductivity.

* Corresponding author. Tel.: +44 20 7882 3235; fax: +44 20 7882 7794.
** Corresponding author.
E-mail addresses: I.Abrahams@qmul.ac.uk (I. Abrahams), fkrok@mech.pw.edu.pl (F. Krok).

0378-7753/$ – see front matter © 2007 Elsevier B.V. All rights reserved.
doi:10.1016/j.jpowsour.2007.05.045

There has been some concern regarding the stability of Bi_2O_3-based electrolytes [16]. Ageing phenomena have been observed in rare earth doped Bi_2O_3 and have been associated with oxide ion redistribution between 8c and 32f sites [17,18]. In the present work, we investigate the effects of prolonged annealing at intermediate temperatures in the Bi_3NbO_7–Bi_3YO_6 system.

2. Experimental

2.1. Sample preparations

Samples of $Bi_3Nb_{1-x}Y_xO_{7-x}$ ($x = 0.4$ and 0.6) were prepared using appropriate amounts of Bi_2O_3 (Aldrich, 99.9%), Y_2O_3 (Aldrich, 99.99%) and Nb_2O_5 (Aldrich, 99.9%). Starting mixtures were ground in ethanol using a planetary ball mill. The dried mixtures were heated initially at 740 °C for 24 h, then cooled and reground. The powders were then sintered at 800 °C for 10 h. Samples were slow cooled in air to room temperature over a period of approximately 12 h.

2.2. Ageing

The effects of annealing were investigated at two temperatures. Powdered samples were initially reheated to the sintering temperature for 1 h before slow cooling in the furnace to the appropriate annealing temperature. Samples were annealed in air at 410 and 550 °C for 430 and 500 h, respectively and subsequently slow cooled to room temperature.

2.3. Crystallography

X-ray powder diffraction data were collected at various temperatures on a Philips X'Pert X-ray diffractometer using graphite monochromated Cu Kα radiation ($\lambda_1 = 1.54056$ Å and $\lambda_2 = 1.54439$ Å) fitted with and X'cellerator detector. Data were collected in flat plate θ/θ geometry on a Pt sample holder. Calibration was carried out with an external Si standard. Room temperature data were collected in the 2θ range 10–60°, in steps of 0.008°, with a scan time of 25 s per step.

Powder neutron diffraction data for $Bi_3Nb_{0.6}Y_{0.4}O_{6.6}$ and $Bi_3Nb_{0.6}Y_{0.6}O_{6.4}$ annealed at 410 °C were collected on the Polaris diffractometer at the ISIS facility, Rutherford Appleton Laboratory. Data collected on back-scattering (C-bank, 145°) and low angle (A-bank, 35°) detectors over the respective time of flight ranges 1.0–20 and 0.5–20 ms were used in subsequent refinements. The samples were contained in cylindrical 11 mm diameter vanadium cans located in front of the back-scattering detectors. Data collections of *ca.* 250 μA suitable for defect structure analysis were collected at room temperature for both samples. In addition, short scans of 30 μA were collected at 50 °C intervals over the temperature range 350–700 °C for the $x = 0.4$ sample.

Powder neutron diffraction data for $Bi_3Nb_{0.6}Y_{0.4}O_{6.6}$ and $Bi_3Nb_{0.6}Y_{0.6}O_{6.4}$ annealed at 550 °C were collected on the GEM diffractometer at the ISIS facility, Rutherford Appleton Laboratory. Data collected at room temperature on the 63.62, 91.37 and 154.46° detectors were used in subsequent refinements with samples contained in cylindrical 11 mm diameter vanadium cans. Data collection times of 30 min were used in each case.

Structure refinement was carried out by Rietveld whole profile fitting using the program GSAS [19]. Where appropriate, X-ray and neutron data were used in a combined refinement. A cubic subcell model in space group *Fm*-3*m* was used for all refinements, Bi, Y and Nb were located on the ideal 4a site (0, 0, 0) with oxide ions distributed over three sites; 8c at (0.25, 0.25, 0.25); 32f at approximately (0.3, 0.3, 0.3) and 48i at around (0.5, 0.2, 0.2) [15]. A total occupancy constraint was applied to the oxide ion distribution using the method of Joubert et al. [20].

2.4. Electrical measurements

Electrical parameters were determined by ac impedance spectroscopy up to *ca.* 800 °C using a fully automated Solartron 1255/1286 system in the frequency range 1 Hz to 5×10^5 Hz. Samples for impedance measurements were prepared as rectangular blocks (*ca.* 6 mm × 3 mm × 3 mm) cut from slow cooled sintered pellets using a diamond saw. Platinum electrodes were sputtered by cathodic discharge. Impedance spectra were carried out over two cycles of heating and cooling and collected at programmed temperatures after 15 min of temperature stabilisation. Impedance at each frequency was measured repeatedly until consistency (2% tolerance in drift) was achieved or a maximum number of 25 repeats had been reached.

3. Results and discussion

The X-ray diffraction patterns confirmed that on ageing the samples maintained the basic cubic fluorite structure, with no obvious differences apparent between aged and freshly prepared samples. Fitted neutron diffraction profiles for the aged samples are presented in Figs. 1 and 2, with the corresponding fitted parameters presented in Table 1.

In the neutron diffraction profiles for the $x = 0.4$ composition, superlattice peaks are clearly evident for example in the region 2.0–3.0 Å. These are commonly observed in the Bi_2O_3–Nb_2O_5 system [8–12]. The superlattice ordering appears unchanged on annealing at 410 and 550 °C at this composition. However as we have previously observed in unannealed samples of this composition, the superlattice disappears at around 750 °C and is replaced by a broad background feature characteristic of a local ordering of defects [15]. At the $x = 0.6$ composition, unannealed samples [15] as well as samples annealed at 410 °C show no superlattice ordering, only a broad background feature. Interestingly on annealing at 550 °C, peaks characteristic of a superlattice do appear. However, the superlattice ordering is different to that observed at $x = 0.4$.

In Table 2, the refined oxide ion occupancy on each of the three sites 8c, 32f and 48i is presented as a percentage of total oxide ion content per cell and compared to the values for unannealed samples [15]. The results for $Bi_3Nb_{0.6}Y_{0.4}O_{6.6}$ show that on annealing at 410 °C the occupancy of the 32f site increases at the expense of that of the 8c site, while the occupancy of the 48i

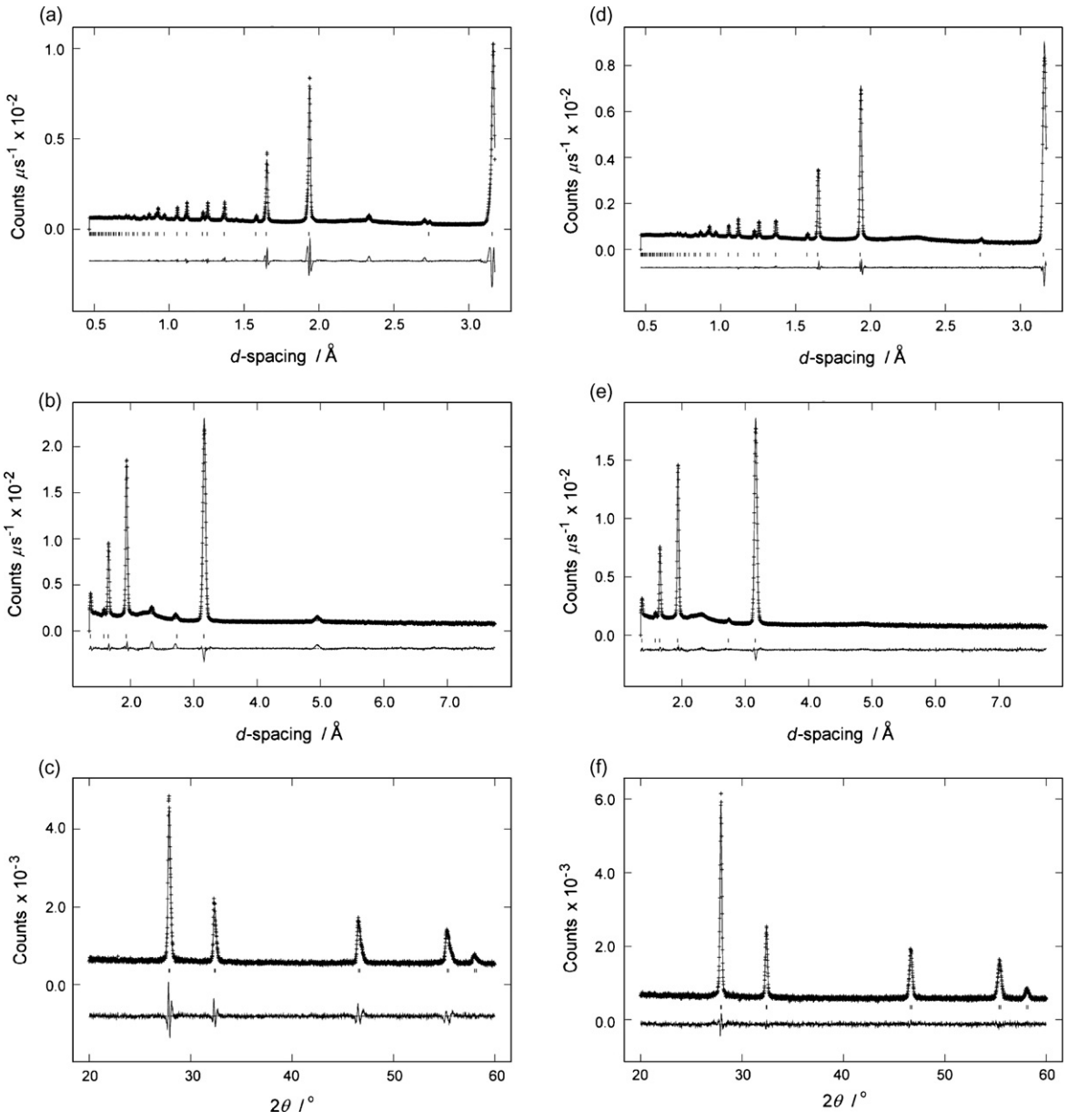

Fig. 1. Fitted diffraction patterns for $Bi_3Nb_{0.6}Y_{0.4}O_{6.6}$ (a–c) and $Bi_3Nb_{0.4}Y_{0.6}O_{6.4}$ (d–f) annealed at 410 °C showing observed (+), calculated (line) and difference (lower) profiles. Reflection positions are indicated by markers: (a and d) neutron (Polaris C-bank, 145°); (b and e) neutron (Polaris A-bank, 35°); (c and f) X-ray data.

site remains almost constant. This trend is maintained on annealing at 550 °C with zero occupancy of the 8c site. Attempts to refine oxygen scattering on the 8c site always resulted in zero or negative occupancies. Similar changes in oxide ion distribution are seen in measurements at 800 °C on freshly prepared samples, with an increase in 32f site occupancy at the expense of that of 8c [15]. In contrast, annealing $Bi_3Nb_{0.4}Y_{0.6}O_{6.4}$ at 410 °C results in very little change in oxide ion distribution compared to the situation in unannealed samples. However, increasing the annealing temperature to 550 °C does promote an oxide ion redistribution similar to that seen in $Bi_3Nb_{0.6}Y_{0.4}O_{6.6}$. After annealing $Bi_3Nb_{0.4}Y_{0.6}O_{6.4}$ at this higher temperature, zero occupancy is again found for the 8c position with the majority of scattering found in the 32f site. The occupancy of the 48i site also increases slightly in comparison to the situation in unannealed samples, but is comparable to the amount found at 800 °C for the same composition [15].

Arrhenius plots of conductivity for samples in the $Bi_3Nb_{1-x}Y_xO_{7-x}$ series generally show a linear low temperature region with the onset of non-Arrhenius behaviour evident at temperatures above *ca.* 500 °C. At the two compositions, $x = 0.4$ and $x = 0.6$, the curvature is towards a region of lower activation energy at higher temperatures (Fig. 3). We have previously correlated this curvature with a temperature dependency of the oxide ion distribution, which additionally exhibits compositional dependence [14,15]. The lower activation energy at higher temperatures is correlated with an increase in oxide ion occupancy of the 32f site at the expense of that of 8c as evi-

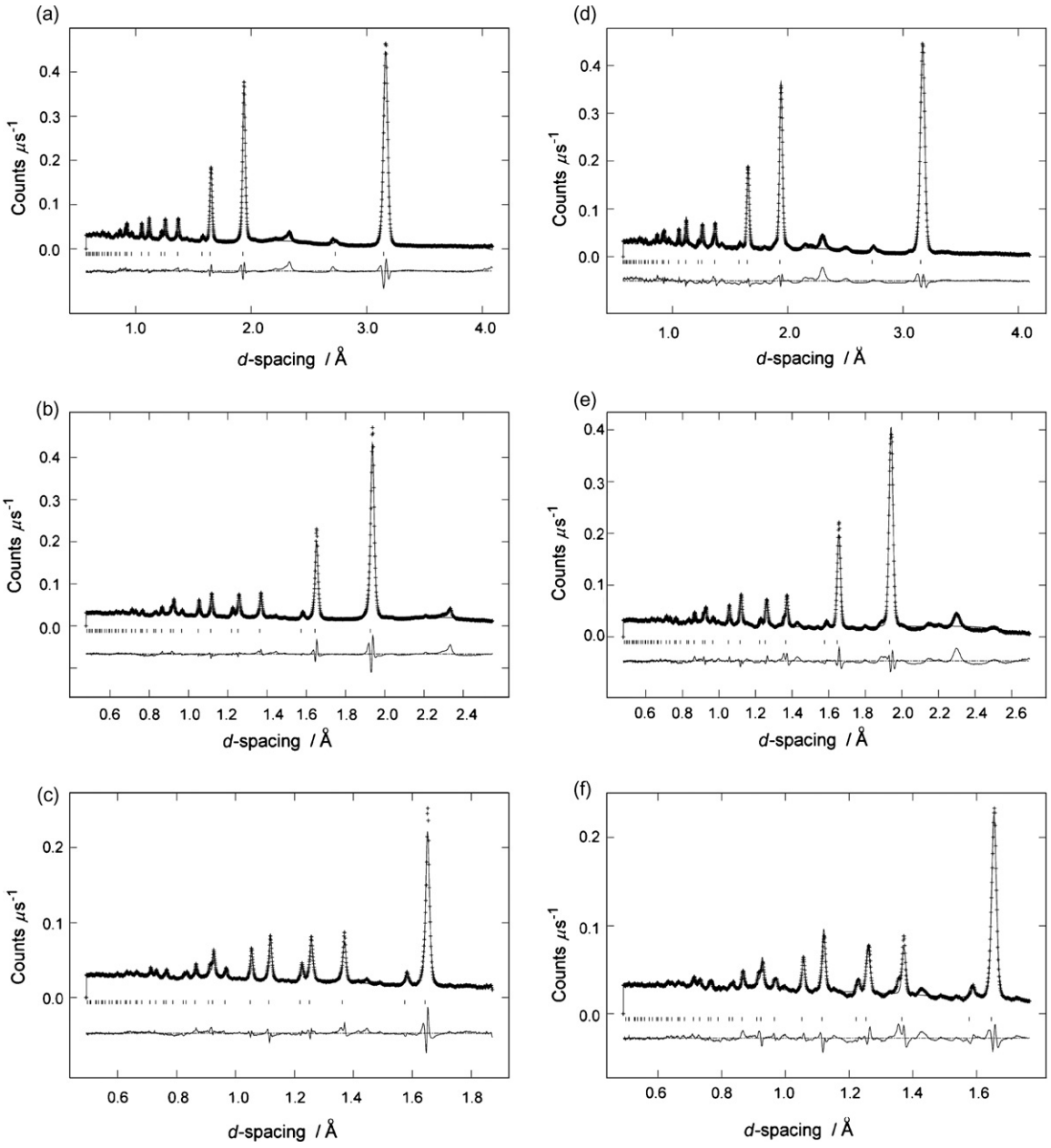

Fig. 2. Fitted neutron diffraction patterns for $Bi_3Nb_{0.6}Y_{0.4}O_{6.6}$ (a–c) and $Bi_3Nb_{0.4}Y_{0.6}O_{6.4}$ (d–f) annealed at 550 °C showing observed (+), calculated (line) and difference (lower) profiles. Reflection positions are indicated by markers: (a and d) GEM bank 4 (63.62°); (b and e) GEM bank 5 (91.37°); (c and f) GEM bank 6 (154.46°).

denced in neutron diffraction results. The 32f site lies very close to the 8c site, but is very likely to be on the conduction pathway and hence ions located in this site have a lower activation energy for conduction than those located in the ideal 8c site.

The higher annealing temperature of 550 °C lies within the curved region of the Arrhenius plots for both compositions studied (Fig. 3). At this temperature both samples exhibit appreciable oxide ion conductivities ($\sigma_{550} = 6.4 \times 10^{-3}$ and 2.1×10^{-2} S cm^{-1} for $x = 0.4$ and $x = 0.6$, respectively) indicative of high oxide ion mobility. The present results suggest that annealing at this temperature for extended periods allows for a redistribution of oxide ions away from the 8c site towards the 32f site in a way that resembles the situation at 800 °C. It is likely that the same mechanism of oxide ion redistribution operates at both temperatures, but that the kinetics at 550 °C are much slower than those at 800 °C and therefore require much longer annealing times to achieve similar oxide ion distributions. This suggests that the oxide ion distribution seen in unannealed samples, involving occupation of the 8c site, is a metastable state at 550 °C.

The situation on annealing at 410 °C is different for the two compositions. At the $x = 0.4$ composition, the 8c/32f oxide ion occupancy redistribution follows the same trend as seen at 550 °C, but some residual occupancy of the 8c site is still evident indicative of slower kinetics at this temperature. In contrast, the $x = 0.6$ sample shows an almost unchanged oxide ion distribution

Table 1
Refined structural parameters for samples of $Bi_3Nb_{1-x}Y_xO_{7-x}$ (a) $x = 0.4$ and (b) $x = 0.6$, unannealed and annealed at 410 and 550 °C

	Unannealed	Annealed 410	Annealed 550
(a) $x = 0.4$			
a (Å)	5.4811(3)	5.4721(9)	5.468774(1)
Bi/Nb/Y, U_{iso} (Å^2)	0.0265(1)	0.0239(2)	0.0227(3)
O1/O2/O3, U_{iso} (Å^2)	0.0694(9)	0.061(1)	0.053(2)
O1 (Occ.)	0.19(2)	0.06(3)	0
O2			
x	0.292(1)	0.289(1)	0.2867(5)
Occ.	0.128(5)	0.161(8)	0.177(1)
O3			
y, z	0.219(2)	0.214(2)	0.275(4)
Occ.	0.020(1)	0.020(1)	0.020(1)
R_{wp}			
	0.0202 (C-bank)	0.0318 (C-bank)	0.1098 (Bank-4)
Neutron	0.0655 (A-bank)	0.0587 (A-bank)	0.0835 (Bank-5)
			0.0667 (Bank-6)
X-ray	0.0932	0.0650	–
All data	0.0331	0.0351	0.0931
(b) $x = 0.6$			
a (Å)	5.4874(3)	5.4698(3)	5.478418(1)
Bi/Nb/Y, U_{iso} (Å^2)	0.0317(1)	0.02982(9)	0.0238(5)
O1/O2/O3, U_{iso} (Å^2)	0.068(1)	0.0634(6)	0.041(2)
O1 (Occ.)	0.26(2)	0.28(1)	0
O2			
x	0.300(1)	0.2989(7)	0.2847(8)
Occ.	0.097(4)	0.105(2)	0.162(1)
O3			
y, z	0.208(2)	0.199(1)	0.311(2)
Occ.	0.017(1)	0.017(1)	0.024(1)
R_{wp}			
	0.0143 (C-bank)	0.0118 (C-bank)	0.0759 (Bank-4)
Neutron	0.0410 (A-bank)	0.0350 (A-bank)	0.1012 (Bank-5)
			0.0885 (Bank-6)
X-ray	0.0961	0.0432	–
All data	0.0289	0.0159	0.0865

in comparison to freshly prepared samples. This suggests that an oxide distribution close to that seen in unannealed samples is the stable state at this temperature.

These results are comparable to those reported by Boyapati et al. on ageing phenomena in rare earth doped bismuth oxide systems of the type $(Bi_2O_3)_{0.75}(Ln_2O_3)_{0.25}$ [17,18]. These authors found that in some systems, for example where Ln = Yb, significant oxide ion redistribution occurred between 8c and 32f sites, while in others, for example where Ln = Dy, a lower degree of oxide ion redistribution occurred. They explained this in terms of the differing ionic radii and polarizabilities of the dopants.

Table 2
Oxide ion distribution on 8c, 32f and 48i sites presented as percentage of total oxide ion scattering per cell in $Bi_3Nb_{1-x}Y_xO_{7-x}$ (a) $x = 0.4$ and (b) $x = 0.6$, unannealed and annealed at 410 and 550 °C

Site	Unannealed	Annealed 410	Annealed 550
(a) $x = 0.4$			
8c	23.4	7.4	0
32f	61.9	77.9	85.6
48i	14.7	14.6	14.4
(b) $x = 0.6$			
8c	38.3	35	0
32f	48.7	52.5	81.7
48i	13	12.5	18.3

The variation in unit cell parameters with temperature for the $x = 0.4$ composition annealed at 410 °C is compared to that in the unannealed sample in Fig. 4. Both samples show non-linear behaviour, which in the case of the unannealed sample can be correlated with the curvature seen in the Arrhenius plot of conductivity and is attributed to a gradual redistribution of oxide ions between 8c and 32f sites. It is interesting to note that the difference in cell dimensions between the annealed and unannealed samples decreases with increasing temperature. This suggests that the differences seen in the room temperature oxide ion distribution between these samples is reduced on heating to higher temperatures and implies that at high temperatures the oxide ion distribution is independent of thermal history.

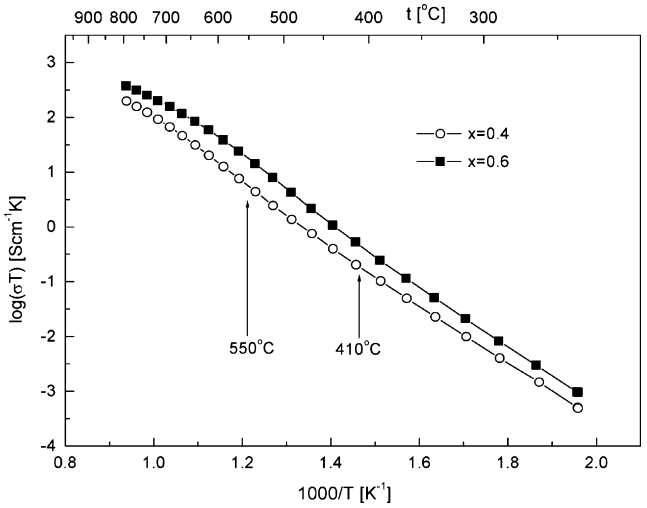

Fig. 3. Arrhenius plots of total conductivity for compositions in the $Bi_3Nb_{1-x}Y_xO_{7-x}$ system, $x=0.4$ and $x=0.6$. Only first cooling curves are shown. Annealing temperatures are indicated.

3.1. Defect structure

The defect structure of compositions in the $Bi_3Nb_{1-x}Y_xO_{7-x}$ system is closely related to that in the parent δ-Bi_2O_3. A number of different models have appeared describing the defect structure in δ-Bi_2O_3 and can be differentiated by differences in the oxide ion distributions over the 8c and 32f sites [21–25]. These two sites lie in close proximity to one another and it is often difficult to unambiguously distinguish scattering from the two sites. Nevertheless, using high quality diffraction data it is possible to refine separate oxide ion occupancies for these two sites, although the coupling of isotropic thermal parameters is typically required. The importance of distinguishing scattering from these two sites lies in the fact that oxide ions located in these sites exhibit different coordination numbers. Ions located in the ideal fluorite 8c site coordinate to four equidistant cations (at around 2.3 Å in δ-Bi_2O_3) in a regular tetrahedral geometry. The 32f site, is displaced from the 8c site by a shift in the ⟨1 1 1⟩ direction, which causes ions in the 32f site to be closer to three cations resulting in a trigonal pyramidal geometry with a fourth non-bonding cation contact (2.7 Å in δ-Bi_2O_3). As a consequence, occupation of the 32f site reduces the cation coordination number. For example in δ-Bi_2O_3 the average coordination number for Bi ranges from 4.5 (for exclusive occupation of 32f sites) to 6 (for exclusive occupation of 8c sites) depending on the model used. In the most recent study of δ-Bi_2O_3 occupancy of both 8c and 32f sites is seen and the average Bi coordination number can be calculated as 5.02 [25].

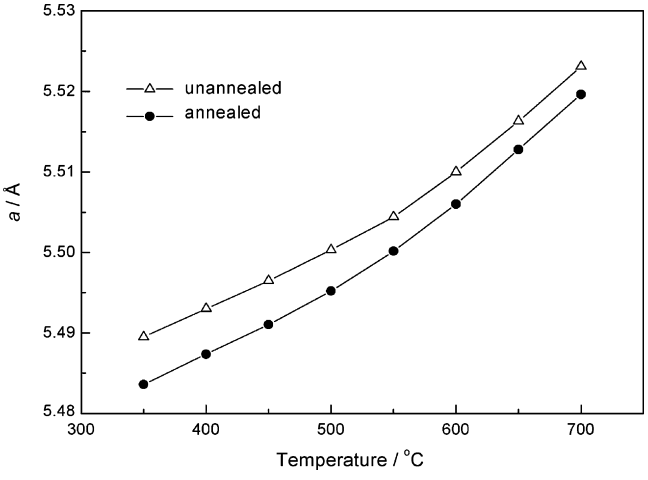

Fig. 4. Temperature variation of cubic unit cell parameter in $Bi_3Nb_{0.6}Y_{0.4}O_{6.6}$, showing data for an unannealed sample and a sample annealed at 410 °C for 430 h.

In the present study, there is additionally occupation of the 48i site, O(3). Oxide ions located in this site coordinate two cations in an angular geometry. Since occupation of this site only appears to occur in substituted bismuth oxides it is reasonable to suppose that oxide ions in this site are associated with coordination to the substituent atom. From the data in Table 2 the ratio of oxide ions in the 48i site to the combined Nb/Y content is close to 1:1. If it is assumed that O(3) is exclusively associated with Nb/Y, then the approximate ratio of 1:1 for O(3):(Nb/Y) means that each Nb/Y atom is coordinated to two shared O(3) atoms. A coordination number of 6 for Nb was recently reported in the structure of the closely related composition, $Bi_{94}Nb_{32}O_{221}$ [12]. Indeed, the crystal chemistry of niobium oxides is dominated by this coordination number. Similarly yttrium usually adopts six coordination in oxides, although higher coordination numbers are also possible. Therefore Nb/Y atoms additionally require coordination to oxide ions in the 32f sites or 8c sites. Six coordination for Nb was recently proposed in the tungsten doped analogue $Bi_3Nb_{0.8}W_{0.2}O_{7.1}$ [26].

4. Conclusions

Annealing at intermediate temperatures can have a significant effect on oxide ion distribution in the system $Bi_3Nb_{1-x}Y_xO_{7-x}$. The effect manifests itself through a shift in oxide ion scattering from the ideal fluorite site 8c to the displaced site 32f. This is typically accompanied by a small reduction in lattice parameter. On annealing at 550 °C for prolonged periods, this change in oxide ion distribution is complete with no observable occupancy of the 8c site. At the $x=0.6$ composition annealing at 550 °C for prolonged periods results in the appearance of a superstructure, more characteristic of lower x-value compositions. Comparison of unit cell parameter variation with temperature for annealed and unannealed samples indicates that at higher temperatures the oxide ion distribution is independent of thermal history.

References

[1] T. Takahashi, H. Iwahara, Y. Nagaj, J. Appl. Electrochem. 2 (1972) 97.
[2] G. Mairesse, in: B. Scrosati, A. Magistris, C.M. Mari, G. Mariotto (Eds.), Fast Ion Transport in Solids, Kluwer Academic Publishers, Dordrecht, 1993, p. 271.
[3] J.C. Boivin, G. Mairesse, Chem. Mater. 10 (1998) 2870.
[4] P. Shuk, H.D. Wiemhöfer, U. Guth, W. Göpel, M. Greenblatt, Solid State Ionics 89 (1996) 179.
[5] N.M. Sammes, G.A. Tompsett, H. Näfe, F. Aldinger, J. Eur. Ceram. Soc. 19 (1999) 1801.
[6] A.M. Azad, S. Larose, S.A. Akbar, J. Mater. Sci. 29 (1994) 4135.

[7] J.B. Goodenough, A. Manthiram, M. Paranthaman, Y.S. Zhen, Mater. Sci. Eng. B 12 (1992) 357.
[8] W. Zhou, D.A. Jefferson, J.M. Thomas, Proc. Roy. Soc. London, Ser. A 406 (1986) 173.
[9] C.D. Ling, R.L. Withers, S. Schmid, J.G. Thompson, J. Solid State Chem. 137 (1998) 42.
[10] A. Castro, E. Aguado, J.M. Rojo, P. Herrero, R. Enjalbert, J. Galy, Mater. Res. Bull. 33 (1998) 31.
[11] R.L. Withers, C.D. Ling, S. Schmid, Z. Kristallogr. 214 (1999) 296.
[12] C.D. Ling, M. Johnson, J. Solid State Chem. 177 (2004) 1838.
[13] F. Krok, I. Abrahams, W. Wrobel, S.C.M. Chan, A. Kozanecka, T. Ossowski, Solid State Ionics 175 (2004) 335.
[14] A. Kozanecka-Szmigiel, F. Krok, I. Abrahams, W. Wrobel, S.C.M. Chan, J.R. Dygas, Mater. Sci. Pol. 24 (2006) 31–37.
[15] I. Abrahams, A. Kozanecka-Szmigiel, F. Krok, W. Wrobel, S.C.M. Chan, J.R. Dygas, Solid State Ionics 177 (2006) 1761.
[16] A. Watanabe, K. Das, J. Solid State Chem. 163 (2002) 224.
[17] S. Boyapati, E.D. Wachman, N. Jiang, Solid State Ionics 140 (2001) 149.
[18] S. Boyapati, E.D. Wachman, B.C. Chakoumakos, Solid State Ionics 138 (2001) 293.
[19] A.C. Larson, R.B. Von Dreele, Los Alamos National Laboratory Report No. LAUR-86-748, 1987.
[20] J.-M. Joubert, R. Cerny, M. Latroche, A. Percheron-Gueqan, K. Yvon, J. Appl. Crystallogr. 31 (1998) 327.
[21] G. Gattow, H. Schroeder, Z. Anorg. Allgem. Chem. 318 (1962) 176.
[22] F. Hund, Z. Anorg. Allgem. Chem. 333 (1964) 248.
[23] H.A. Harwig, Z. Anorg. Allgem. Chem. 444 (1978) 151.
[24] P.D. Battle, C.R.A. Catlow, J. Drennan, A.D. Murray, J. Phys. C 16 (1983) L561.
[25] M. Yashima, D. Ishimura, Chem. Phys. Lett. 378 (2003) 395.
[26] I. Abrahams, F. Krok, S.C.M. Chan, W. Wrobel, A. Kozanecka-Szmigiel, A. Luma, J.R. Dygas, J. Solid State Electrochem. 10 (2006) 569.